Supplementary Materials

for

"A New Year's Day Icebreaker: Icequakes on Lakes in Alberta, Canada"

Jeffrey Kavanaugh, Ryan Schultz, Laurence Andriashek,

Mirko van der Baan, Hadi Ghofrani, Gail Atkinson, Dan Utting

Canadian Journal of Earth Sciences

Includes: Supplementary Methods, Table S1, References, and Figures S1-S7.

Supplementary Methods

Ice temperature model description

To examine temperature conditions within the lake ice and overlying snow cover, we developed a simple mathematical model that solves the evolution of the temperature *T* at height *z* above the base of the lake ice with time *t*:

$$\frac{\partial T}{\partial t} = \frac{1}{\rho c(T)}\left[K(T)\frac{\partial^2 T}{\partial z^2} + K'(T)\frac{\partial T}{\partial z}\frac{\partial T}{\partial z}\right] \quad \text{(Eq. S1)}$$

Here $\partial T/\partial z$ and $\partial^2 T/\partial z^2$ are the first and second spatial derivatives of temperature and ρ, $c(T)$, and $K(T)$ are, respectively, the density, heat capacity, and specific heat of the ice or snow. This expression was developed from the energy balance equation and Fourier's law of heat conduction, with the assumptions of no internal energy source and negligible strain heating. Formulae used for the heat capacity and thermal conductivity of ice are from Cuffey and Paterson (2010):

$$c(T) = 152.5 + 7.122T \quad \text{(Eq. S2)}$$

$$K_I(T) = 9.828\exp(-5.7 \times 10^{-3}T) \quad \text{(Eq. S3)}$$

So defined, K_I' $(= \partial K_I/\partial T)$ is:

$$K_I'(T) = -5.60 \times 10^{-2}\exp(-5.7 \times 10^{-3}T) \quad \text{(Eq. S4)}$$

In these three equations, the temperature *T* is in Kelvin; each is expressed in appropriate S.I. units. The expression used for the thermal conductivity of snow is from Van Dusen (1929):

$$K_S(\rho) = 2.1 \times 10^{-2} + 4.2 \times 10^{-4}\rho + 2.2 \times 10^{-9}\rho^3 \quad \text{(Eq. S5)}$$

As the thermal conductivity of snow is a function of density, rather than temperature, $K_S' = 0$.

Equation S1 was solved using the method of lines (e.g. Schliesser, 1991), in which the spatial derivatives are treated as a finite difference problem and the resulting set of coupled ODEs are solved numerically (here by the MATLAB™ solver ode45, which implements a Runge-Kutta method with variable timestep). Fourth-order finite difference expressions used for the first and second spatial derivatives in the vertical temperature profile are from Schliesser (1991), and temperatures at the top and bottom of the model domain are prescribed. The model is initialized by assuming that temperatures vary linearly with depth, and the model is allowed to proceed until a steady-state condition is met, after which the time is reset to zero and the prescribed air temperature and snow cover scenarios described in the manuscript are run.

Following completion of each temperature/snow cover scenario, the change in depth-averaged ice temperature $\overline{\Delta T}$ over the modelled time is calculated. This value is used to determine the amount of thermal expansion ΔL of the ice, as given by:

$$\Delta L = \overline{\Delta T} \alpha_I L \qquad \text{(Eq. S6)}$$

Here α_I is the coefficient of linear expansion of ice and L the approximate radius of Lac Ste. Anne. Relevant model parameter values are given in Table S1.

Table S1. List of parameters used in ice modelling.

Parameter	***Value***
Ice density, ρ_I	$917\ \mathrm{kg/m^3}$
Snow density, ρ_S	$330\ \mathrm{kg/m^3}$
Coefficient of linear expansion of ice, α_I	$5.0 \times 10^{-5}\ \mathrm{K^{-1}}$
Radius of Lac Ste. Anne, L	5.0 km
Water temperature	0°C
Air temperature (initial)	−30°C
Ice thickness	0.4 m

Snow thickness	0.0 m or 0.3 m
Model node spacing	0.01 m
Maximum fractional misfit (for steady-state solution)	1×10^{-9}

Supplementary References

Cuffey, K.M., and W.S.B. Paterson. 2010. *The Physics of Glaciers*. 4th ed., Butterworth-Heinemann/Elsevier, Burlington, MA.

Schliesser, W.E. 1991. *The Numerical Method of Lines: Integration of partial differential equations.* Academic Press, San Diego, CA.

Van Dusen, M.S. Thermal conductivity of non-metallic solids. In: Washburn, E.W. (Ed.), *International Critical Tables of Numerical Data. Physics, Chemistry and Technology, vol. 5.* McGraw Hill, New York, NY.

Supplementary Figures & Captions

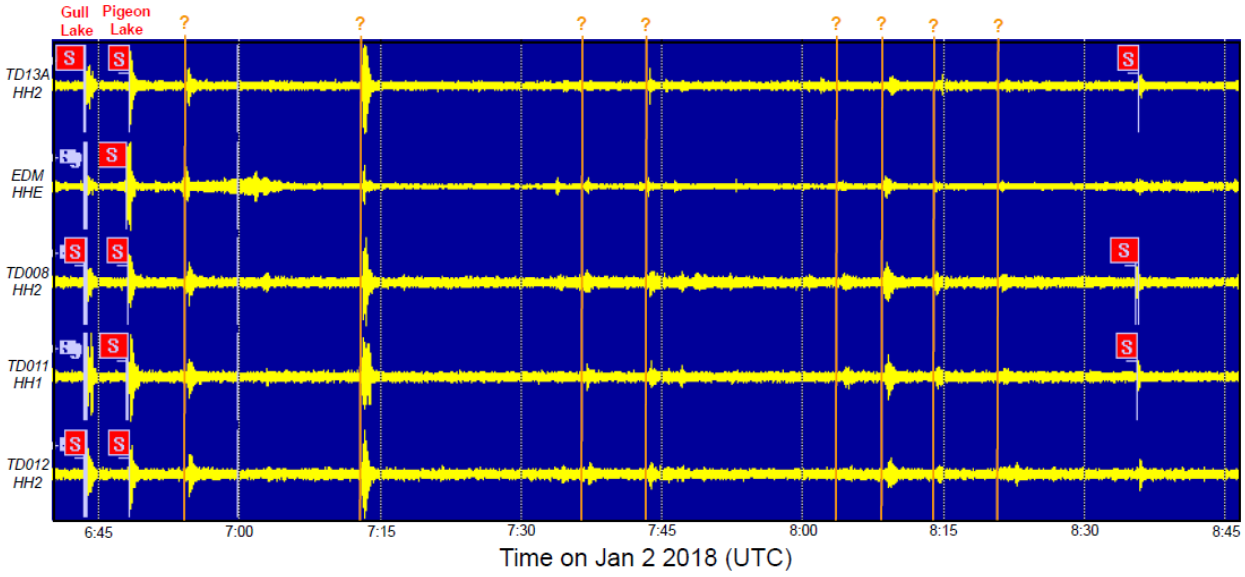

Figure S1. Waveform data during the evening of January 1-2 2018. Horizontal components of waveform data from nearby stations (yellow lines) have been shifted to an origin time/location corresponding to Pigeon Lake. Shear-wave arrivals for the Gull Lake and Pigeon Lake events have been annotated (red S boxes). The presence of arrivals that are too small to be located, but large enough to be detected (vertical orange lines).

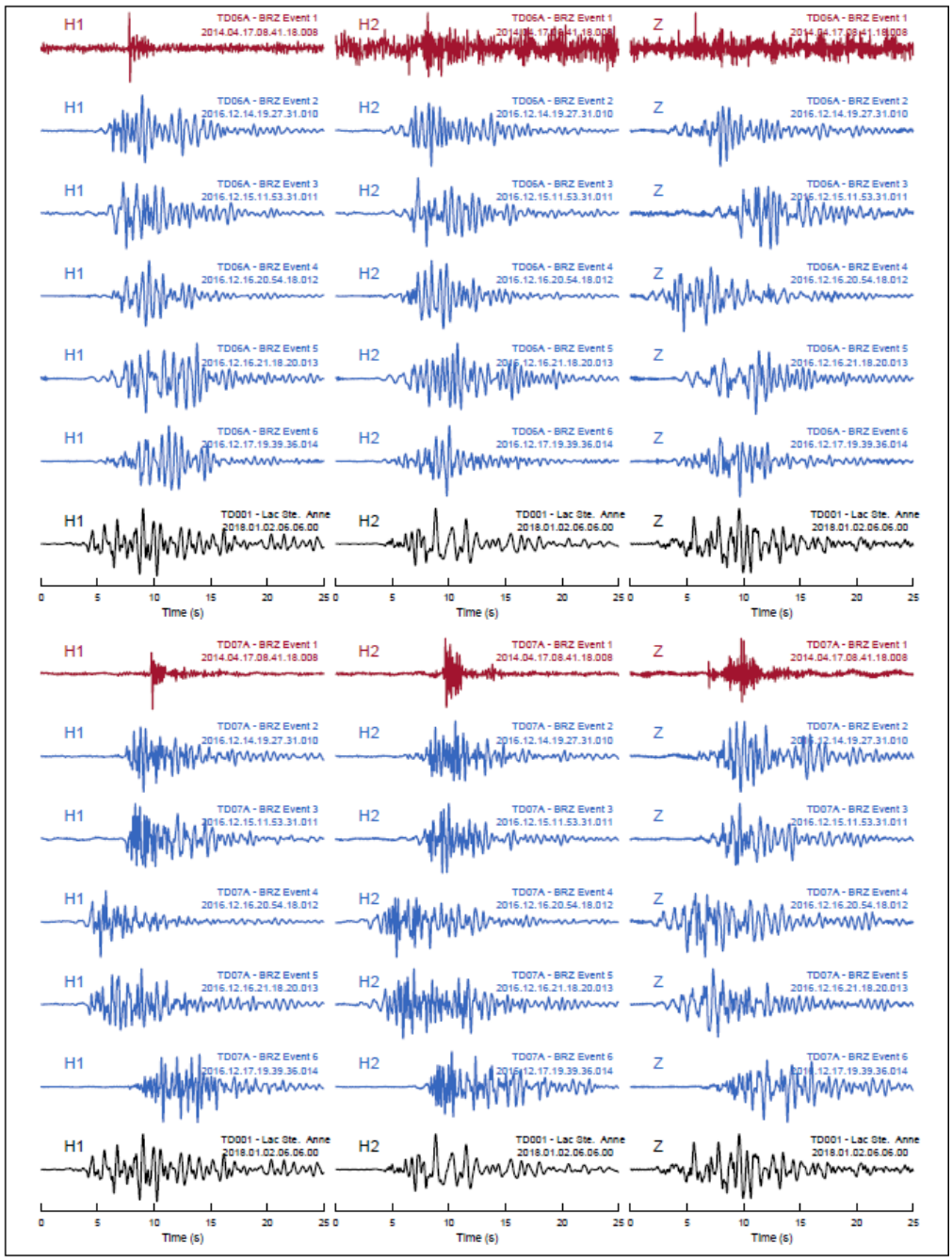

Figure S2. Comparison of seismic event waveforms. Columns from left to right plot horizontal and vertical components of velocity waveforms. The first set of plots show the waveforms from 6 small-magnitude Brazeau events recorded on stations TD06A (top set) and TD07A (bottom set); the small, natural earthquake is Event 1 (red waveforms) and the remaining are cryoseisms (blue waveforms). The waveforms of the Lac Ste. Anne event are in black at the bottom of each set. Distances and station details are included in the corresponding text. All signals are bandpass filtered between 0.5-15 Hz.

Figure S3. More damage to infrastructure. (a & b) Sheared deck structure, Lac Ste. Anne. (c) Sheared lower building structure, Seba Beach area, Wabamun Lake. Note severed electrical conduit and electrical wiring. In all panels, arrows indicate directions of ground displacements. Locations of pictures are annotated in panels based on acronyms in Figure 1.

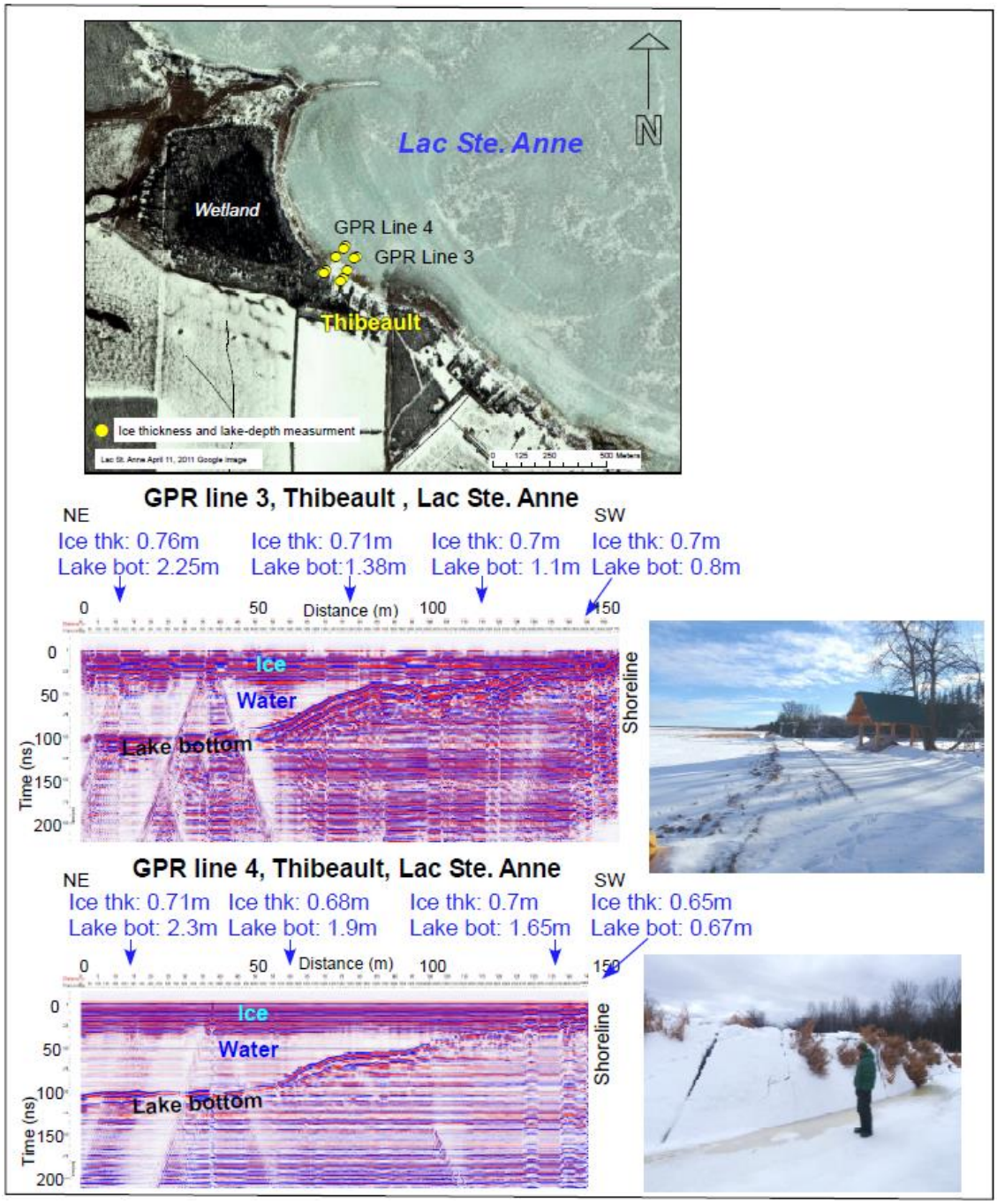

Figure S4. Ground penetrating radar profiles of ice thickness and lake-bottom morphology, Thibeault, Lac Ste. Anne. GPR profiles were surveyed on January 19 2018, about 2.5 weeks after icequake event. Yellow dots in location figure denote ice-auger borehole sites. Blue vertical arrows above GPR profiles denote positions of ice-auger boreholes, and blue text is sounding information at site. Hyperbolic forms expressed to surface denote the location of re-frozen leads in the lake ice.

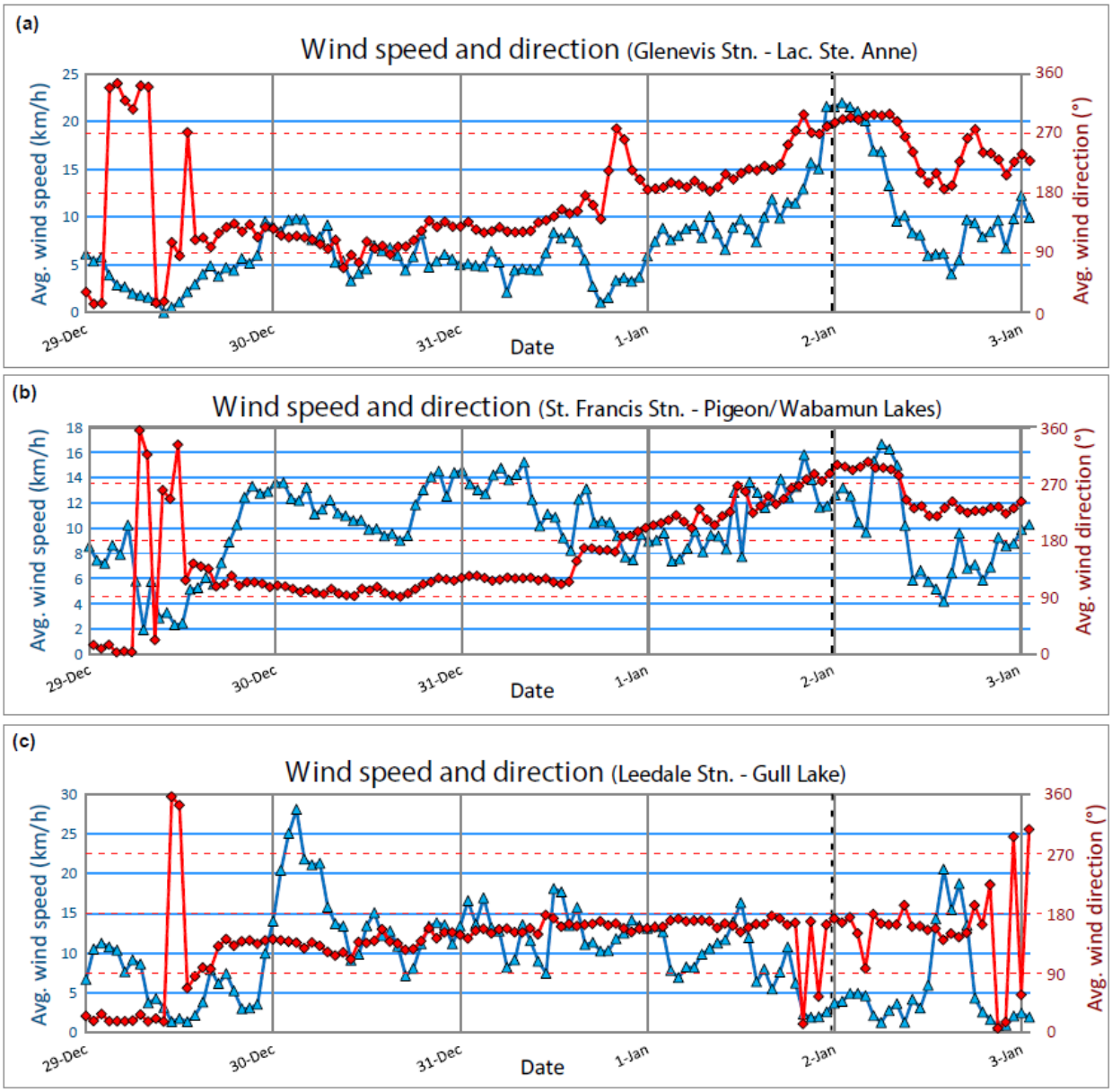

Figure S5. Wind speed and direction data. Wind speed (blue line) and direction (red line) are displayed for a period around the observed seismic events (vertical dashed line) at three weather stations nearby lakes in central Alberta.

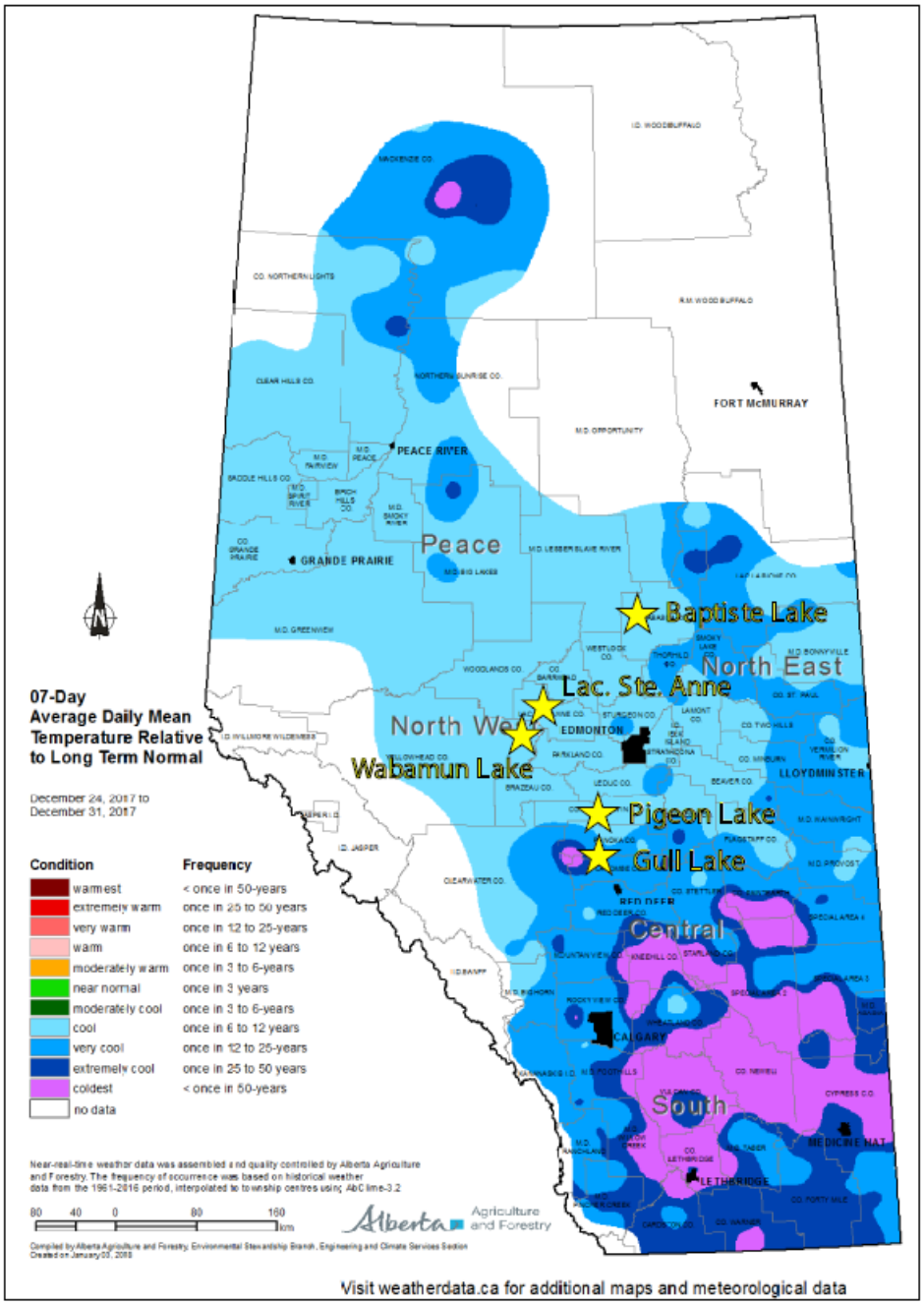

Figure S6. Average daily mean temperature relative to normal in late December 2017. Yellow stars show locations of lakes that registered on seismic monitoring stations, or which experienced ice-ridge and/or ground deformation. Gull Lake, Lac. Ste. Anne, Baptiste Lake, and Wabamun Lake are located in areas that are cooler than the long term average. Base map source: http://agriculture.alberta.ca/acis/climate-maps.jsp.

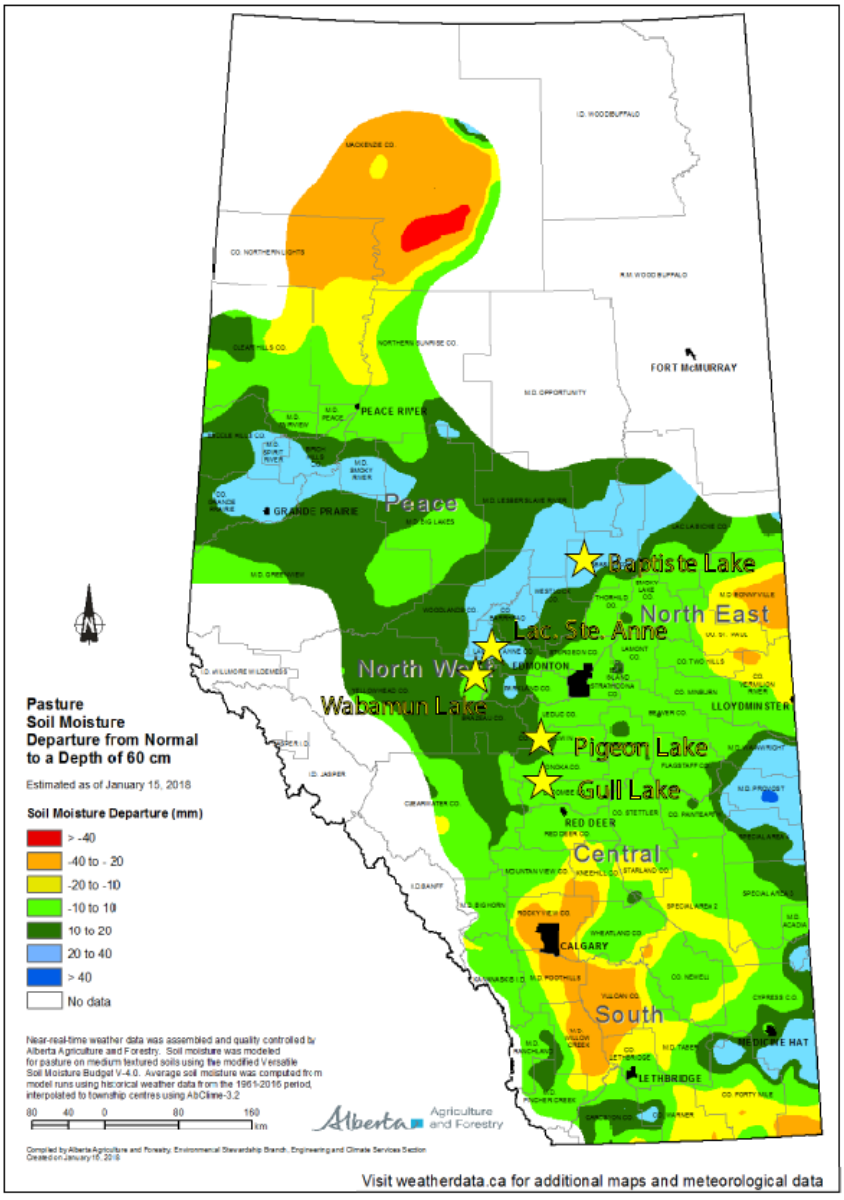

Figure S7. Average soil moisture relative to normal in January 2018. Yellow stars show locations of lakes that registered on seismic monitoring stations, or which experienced ice-ridge and/or ground deformation. Gull Lake, Lac. Ste. Anne, Baptiste Lake, and Wabamun Lake are located in areas that are wetter than the long term average. Base map source: http://agriculture.alberta.ca/acis/climate-maps.jsp.